Chinese Chemical Letters 34 (2023) 107622

Contents lists available at ScienceDirect

Chinese Chemical Letters

journal homepage: www.elsevier.com/locate/cclet

Tuning the hydrogen and hydroxyl adsorption on Ru nanoparticles for hydrogen electrode reactions *via* size controlling

Zhengrong Li, Lulu An, Min Song, Tonghui Zhao, Jingjing Zhang, Chang Zhang, Zhizhan Li, Deli Wang*

Key Laboratory of Material Chemistry for Energy Conversion and Storage, Ministry of Education, Hubei Key Laboratory of Material Chemistry and Service Failure, School of Chemistry and Chemical Engineering, Huazhong University of Science and Technology, Wuhan 430074, China

ARTICLE INFO

Article history:
Received 7 April 2022
Revised 6 June 2022
Accepted 17 June 2022
Available online 22 June 2022

Keywords:
Hydrogen oxidation reaction
Hydrogen evolution reaction
Electrocatalysis
Ruthenium particle
Particle size
Hydrogen binding energy

ABSTRACT

Controlling the particle size of catalyst to understand the active sites is the key to design efficient electrocatalysts toward hydrogen electrode reactions including hydrogen oxidation and evolution (HOR/HER). Herein, the hydrogen and hydroxyl adsorption on Ru/C could be effectively tuned for HOR/HER by simple controlling the particle sizes. It is found that the metallic Ru (Ru^0) is the active site for HOR/HER, while oxidized Ru (Ru^{x+}) will hinder the adsorption and desorption of hydrogen on the catalyst. For the HOR, catalyst with small particles is more efficient, due to it is a three-phase interface reaction of gas on the surface of the catalyst. For the HER, the metallic state of Ru is crucial. The deconvolution of hydrogen peaks indicates that the catalytic sites with low hydrogen binding energy (HBE) shoulder the majority of the HOR activity. CO stripping curve further demonstrates that the stronger hydroxyl species (OH_{ad}) affinity is beneficial to promote the HOR performance. The results indicate that the design of efficient HOR/HER catalyst should focus on the balance between particle size and metallic states.

With the development of hydrogen energy, the two important hydrogen electrode reactions (HOR/HER) have attracted great attention [1–3]. It is found that the HOR catalysts still focus on Pt-based materials and the HOR/HER activities of noble metal (Pt, Pd, Ir, Ru and Rh) fall two orders of magnitude when changing from acid to alkaline electrolyte [4]. Therefore, it is necessary to design alkaline HOR/HER catalysts with high activity and low cost [5–10]. It is important to understand the sluggish kinetics of HOR/HER in alkaline electrolyte to design an efficient catalyst, while the study on non-Pt anode catalyst is limited [7,11]. The hydrogen binding energy (HBE) of Ruthenium (Ru) is similar to Pt, and the cost of Ru is only one third of Pt, which makes Ru as a promising substitutable for Pt catalysts [10,12,13]. Recently, many researches of HOR/HER on Ru-based catalysts were carried out in alkaline electrolyte, but the explicit kinetic study of HOR/HER on Ru-based catalysts is still lack [14–16].

The difference of HOR activity on the metal single crystal surfaces demonstrated that it is a structure sensitive reaction [17]. Size, shape and structure of the nanoparticles have influences on the catalytic performance of HOR [18]. It has been reported that Ru/C with particle size of 3 nm showed the highest catalytic activity for HOR in 0.1 mol/L NaOH electrolyte, due to the unique structure of long-bridge coordinated unsaturated Ru atoms on the surface [19]. The research on the particle size effect of Ru/C catalysts have extensively conducted on CO oxidation and catalytic hydrogenation [20,21], and the most of the research on the effect of HOR particle size mainly focused on Pt. Antoine's group tested HOR performance of Pt/C catalysts with size of 2.5–28 nm. The study found that the Pt nanoparticles with the smallest size have the highest specific activity and mass activity [22]. Sun's group showed the HOR activity on Pt/C have "negative" particle size effect in acid electrolyte that with the particle size increasing, the specific activity increases and the mass activity shows a volcanic trend that first increases and then decreases [23]. Subsequently, Ohyama' group found similar results of the HOR activity on Pt/C in alkaline and acid electrolyte, and the HOR activity of 3 nm Pt/C has the highest activity [19]. Zheng's group reported the HOR/HER performance of Ir/C with particle size of 3–12 nm in alkaline electrolyte, proved that the active sites with the lowest HBE contributed to the HOR/HER activity [24]. Later, Zheng's group found that the HOR activity of Pd/C increases with the particle size increases, having the same trend with the proportion of the lower HBE sites [25]. Numerous experiments point out that the surface sites on the catalysts with different particle size possess different activity. Research on the effect of particle size is beneficial to design non-Pt cata-

* Corresponding author.
E-mail address: wangdl81125@hust.edu.cn (D. Wang).

https://doi.org/10.1016/j.cclet.2022.06.045
1001-8417/

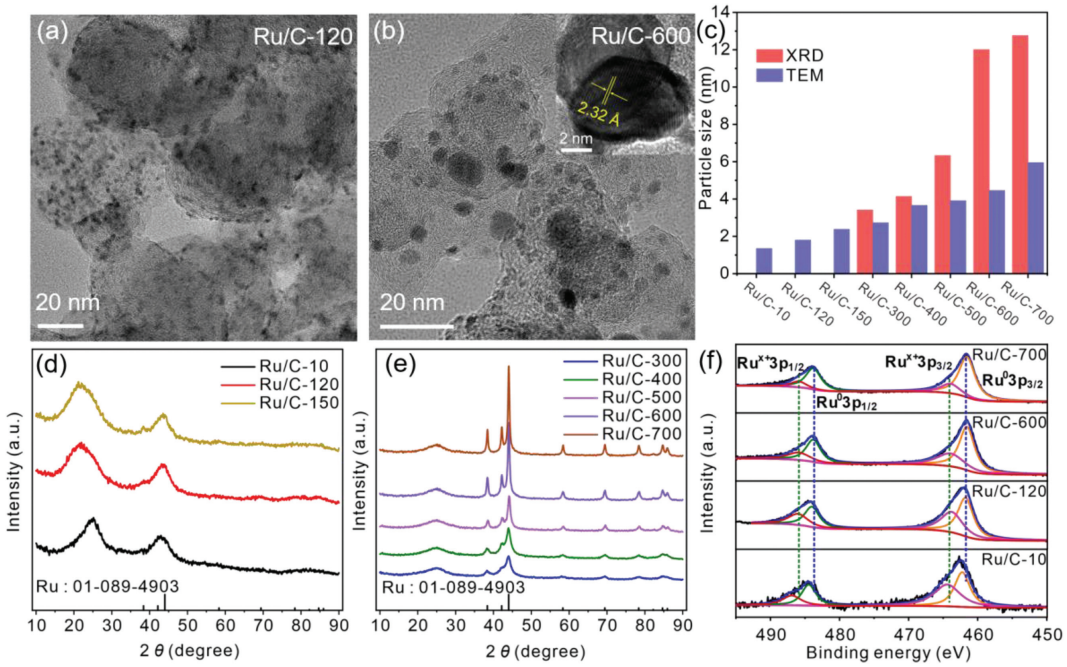

Fig. 1. TEM images of (a) Ru/C-120, (b) Ru/C-600. (c) The particle size calculated from XRD and TEM of all Ru/C samples. (d, e) XRD patterns of all Ru/C samples. (f) Ru 3p high-resolution XPS spectra of Ru/C-10, Ru/C-120, Ru/C-600 and Ru/C-700.

lysts, which is of great significance to the development of anion exchange membrane fuel cells.

Herein, Ru/C with particle sizes varying from 1.35 nm to 5.95 nm supported on Vulcan XC-72 were prepared *via* an impregnation reduction method following heat-treated at different temperature. In alkaline electrolyte, the HOR mass activity presents a volcanic type trend that first increases and then decreases, while the area activity presents an inverted volcanic type trend, with the Ru particle size increasing. The deconvolution of hydrogen peaks shows that active sites with low HBE contribute to most of the catalytic activity, and the adsorption of OH_{ad} can also promote the HOR activity. In addition, it was found that the HER activity showed a volcanic trend that first increased and then decreased with the particle size increases in alkaline electrolyte, but the catalysts with the most excellent HOR and HER performance is not the same. It was further discovered that Ru with a smaller particle size is easier to adsorb oxygenated species in air, due to Ru has a high oxygen affinity. The particle size and surface state of the catalyst affect the HOR/HER activity of the Ru/C catalyst directly, and the effects of these two factors are not the same in the two reactions. This work provides guidance for the subsequent preparation of efficient HOR/HER electrocatalysts.

The particle diameter and distributions of Ru nanoparticles were measured by transmission electron microscopy (TEM). The overview TEM image of Ru/C in Figs. 1a, b and Fig. S1 (Supporting information) demonstrate the Ru particles are well dispersed on the carbon support. Obviously, the size of Ru nanoparticles increases as the annealing temperature increases, due to the Ostwald growth and agglomeration during the annealing treatment [26]. The high resolution TEM (HRTEM) image of the Ru/C-600 in Fig. 1b displays a lattice fringe of 2.32 Å, which can be attributed to the (101) facet of hexagonal Ru [27,28]. The particle size grows from 1.35 nm to 5.95 nm with increasing the temperature (Fig. S2 in Supporting information).

The Ru/C samples were characterized by XRD analysis to reveal the crystal-phase structure. Figs. 1d and e show the XRD patterns of all Ru/C samples. There is no evident characteristic diffraction peak corresponding to Ru species in Ru/C-10, Ru/C-120 and Ru/C-150, indicating that the sample reduced at low temperatures is amorphous structure with small particle size, which is consistent with the TEM results. The Ru/C-300 shows a hexagonal close-packed structure. The peaks at 38.4°, 42.2°, 44.0°, 58.3°, 69.4°, 78.4°, 82.2°, 84.7°, 85.9° are corresponding to (100), (002), (101), (102), (110), (103), (200), (112) and (201) facets of hcp Ru (PDF #01-089-4903), respectively, which indicates that crystalline Ru nanoparticles can be obtained by annealing at 300 °C [27,28]. And with the increasing of annealing temperature, the width of diffraction peaks of Ru becomes narrow, indicating that the particle size tends to increase at a high temperature, consistent with the TEM result. The particle size calculated by XRD patterns are larger than the particles measured by TEM, which is probably due to the polycrystalline structure of the nanoparticles [21]. The particle size is shown in Fig. 1c and Fig. S2 (Supporting information).

The surface component and electronic structure of partial Ru/C catalysts were further characterized by X-ray photoelectron spectroscopy (XPS). Fig. S3 (Supporting information) presents the survey spectra of Ru/C-10, Ru/C-120, Ru/C-600 and Ru/C-700 catalysts, which confirms the presence of Ru, C and O elements in the sample. The surface of Ru is unstable and easy to form surface oxygenated species when exposed to the air [29,30]. The O 1s peak in the survey spectra also verifies the existence of oxide species. The O 1s peak intensity of Ru/C-10 is significantly higher than that of Ru/C-600 and Ru/C-700, indicating that there are more oxide species, which could be related to its small particle size and easy to be oxidized [31]. Owing to the signals of C 1s and Ru 3d overlap at approximately 285 eV, it is more accurate to use Ru 3p for XPS analysis to avoid the interference from carbon [32,33]. The peaks of oxidized state of Ru^{x+} $3p_{3/2}$ and Ru^{x+} $3p_{1/2}$ are centered at ~464.0 eV and ~485.8 eV, respectively. The peaks located at ~461.6 eV and ~483.8 eV could be attributed to the metallic state of Ru^0 $3p_{3/2}$ and Ru^0 $3p_{1/2}$, respectively [28,34]. The binding energy of Ru^0 in Ru/C-10 is much higher than that of Ru/C-700 in Fig. 1f, which also shows that there is a large amount of Ru in oxidative state in Ru/C-10. Fig. S4 (Supporting information) shows the ratio of Ru^0 and Ru^{x+} calculated from the XPS spectra of Ru 3p. It can be obtained that when the annealing treatment temperature

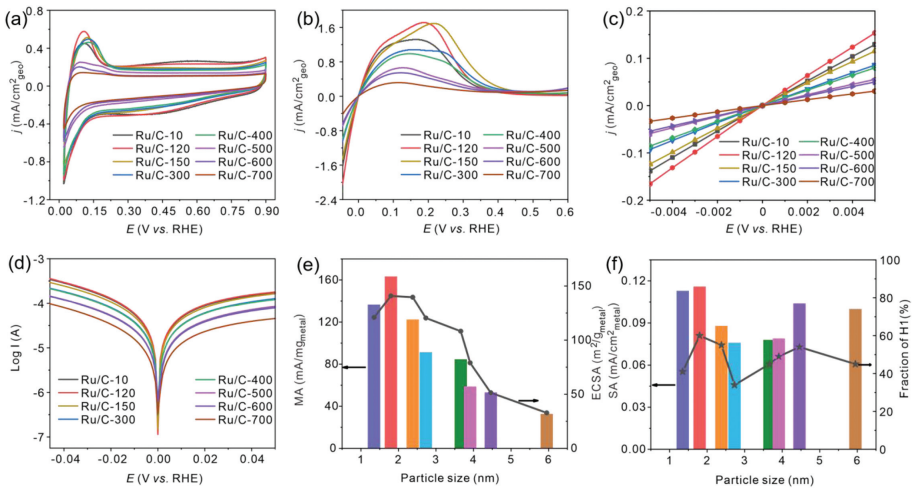

Fig. 2. (a) CV curves, (b) HOR polarization curves, (c) micro-polarization region (−0.005∼0.005 V), (d) Tafel plots of Ru/C catalysts. (e) MA and ECSA of Ru/C catalysts as a function of particle size. (f) Fraction of H1 peaks and SA of all Ru/C catalysts as a function of particle size.

increases, the highest proportion of metallic Ru^0 reached 78.2% for Ru/C-700. Ru/C-10 with the small particle obtained at low temperature has the highest ratio of oxidative state Ru^{x+} (51.6%). It further shows that the Ru/C catalyst with small particle is easy to form oxygenated species when exposed to air, thereby obtaining Ru/C samples with different particle size and surface states.

The cyclic voltammetry (CV) curves of Ru/C catalysts in N_2-saturated 0.1 mol/L KOH were obtained and shown in Fig. 2a. The oxidation peak around 0.12 V of all Ru/C catalysts is attributed to the desorption of the under-potentially deposited hydrogen and the oxidation of Ru surface [19,27,35,36]. With increasing annealing temperature, the electrochemical double layer in the CV curves reduces obviously. And when the reduction temperature reached 500 °C, the hydrogen region of Ru/C-500, Ru/C-600 and Ru/C-700 nearly disappear, due to the decrease of active sites with the growth of particles during the high-temperature annealing [37,38]. The HOR polarization curves of Ru/C catalysts were measured with a rotating disk electrode (RDE) in H_2-saturated 0.1 mol/L KOH. As shown in Fig. 2b, the HOR currents of the Ru/C catalysts increase with the positive scan from −0.05 V to 0.1–0.2 V and then decrease, which corresponds to the CV curve that the hydrogen desorption peaks around 0.1–0.2 V. All of the Ru/C catalysts cannot reach the theoretical diffusion limited current, due to the reason that Ru is easily oxidized and then leads to a lower failure potential [14,15,39,40]. Ru/C-120 shows the smallest polarization overpotential and provides the highest apparent HOR performance among all Ru/C catalysts.

The difference of HOR activity on Ru/C catalysts can be clearly seen from the micro-polarization region and Tafel plots shown in Figs. 2c and d. The Ru/C-120 shows the highest apparent activity, while Ru/C-700 exhibits the lowest activity near the equilibrium potential. The exchange current densities (j_0) cannot be calculated by extrapolating the Tafel curve, due to the reason that Tafel region is unclear, which is caused by the oxidation on the Ru surface [19]. The j_0 is acquired by linear fitting of micro-polarization region (−0.005 V–0.005 V), using the simplified Butler-Volmer equation (Eq. 1) [27,41].

$$j_o = (j/\eta) * (RT/F) \quad (1)$$

where j equals the apparent current density, η is the overpotential, R corresponds to the molar gas constant (8.314 J mol^{-1} K^{-1}), T refers to the Kelvin temperature, and F is the Faraday constant (96,500 C/mol). The calculated j_0 from micro-polarization curves are normalized to the mass of Ru as mass activity (MA). The MA of Ru/C-120 (163.4 mA/mg) is about 1.2 times of that of Ru/C-10 (136.5 mA/mg), and 5 times of that of Ru/C-700 (32.74 mA/mg), indicating the remarkable HOR performance of Ru/C-120. The electrochemical surface areas (ECSA) of all Ru/C catalysts are obtained from CO-stripping voltammetry to further identify intrinsic activities. ECSA of Ru/C catalysts are summarized in Table S1 (Supporting information). Fig. 2e shows the MA and ECSA among these Ru/C catalysts. Generally speaking, the number of active sites decreases with the increase of the particle size in the catalyst [42]. However, as the particle size increases, the ECSA of the Ru/C catalyst first increases and then decreases sharply, which exhibits a volcano type relationship. MA and ECSA have the same trend, and Ru/C-120 has the largest ECSA and the highest MA.

From XPS analysis, the ratio of metallic Ru^0 in Ru/C-10 and Ru/C-120 is 48.4% and 57.4%, respectively. Ru is oxophilic-metal and can be easily oxidized, the metal state of Ru is critical to the high activity of Ru/C for HOR. Although the particle size of Ru/C-10 is smaller than that of Ru/C-120, the ultrafine Ru particles is easily to form surface oxygenated species, which results in a small ECSA of Ru/C-10 than Ru/C-120 as verified in Fig. 1c and Fig. S4 (Supporting information). Since Ru^0 is the active center for HOR, and the existence of the oxygenated species on the surface reduces the number of active sites. In addition, the oxidative state Ru^{x+} inhibits the adsorption of hydrogen, which reduces the electrocatalytic activity of Ru/C-10.

Specific activity (SA) of Ru/C were acquired by normalizing j_0 to ECSA to clarify the intrinsic activities. Fig. 2f depicts the correlation between the SA of Ru/C catalysts, it can be seen that the SA presents an obvious inverted-volcano relationship with the annealing temperature increasing, in which the SA of Ru/C-120 (0.116 mA/cm$^2_{metal}$) is about 1.5 times higher than that of Ru/C-300 (0.076 mA/cm$^2_{metal}$ for the lowest SA). Together with the excellent MA, this demonstrates the excellent intrinsic and apparent performance of Ru/C-120.

Sheng *et al.* found the relationship between the hydrogen binding energies (HBE) or HOR exchange current densities of Pt, Pd, Ir, Rh and pH values is generally monotonically decreased, indicating that HBE might be the dominant descriptor for hydrogen electrode reactions [5,43]. The anodic oxidation peak in the hydrogen desorption region could be assigned to the oxidation of H intermediates (H_{ad}) adsorbed on the crystal faces of Pt, Pd, Ir, Rh, so as Ru [44]. Thus, the hydrogen desorption region of Ru/C were di-

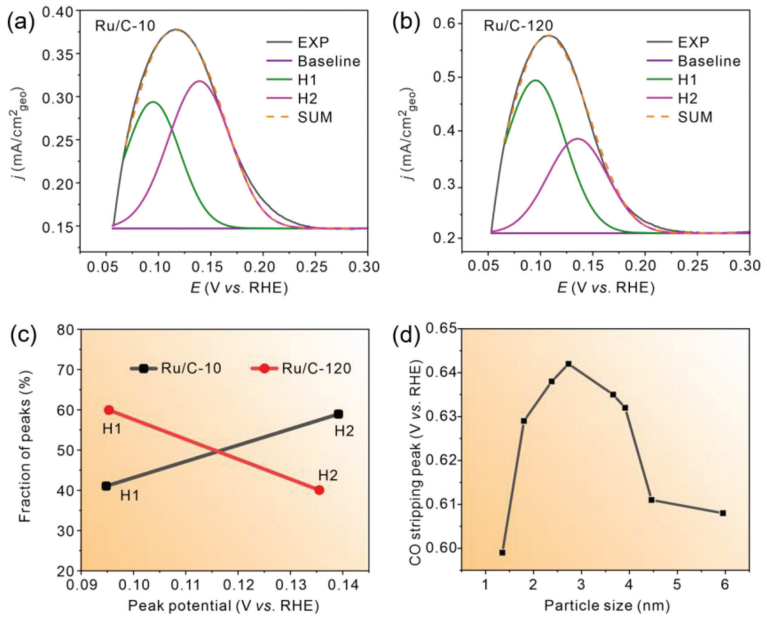

Fig. 3. Divide hydrogen region into two peaks centered at 0.090–0.095 V (H1) and 0.135–0.139 V (H2) for (a) Ru/C-10 and (b) Ru/C-120. (c) The fraction of H1 and H2 in Ru/C-10 and Ru/C-120. (d) CO stripping peak of Ru/C catalysts.

vided into two peaks, to establish the relationship between the active sites distribution and catalytic performance, that the negative anode peak corresponding to lower HBE.

The deconvolution of hydrogen desorption peaks of Ru/C-10 and Ru/C-120 are shown in Fig. 3. Ru/C-10 has two peaks at 0.095 V (H1) and 0.139 V (H2) for the proportion of 41.05% and 58.95%, correspondingly. While for Ru/C-120, the H1 and H2 peaks negatively shift to 0.090 and 0.135 V, with the proportion of 59.94% and 40.06%. The peak of hydrogen desorption is closer to the equilibrium potential, indicating that the desorption of H_{ad} is easier, and the active site has higher catalytic activity for HOR. Obviously, both deconvolution peaks of Ru/C-120 are closer to the equilibrium potential than that of Ru/C-10. Furthermore, the proportion of H1 in Ru/C-120 is remarkably higher than that in Ru/C-10, indicating that there are more highly active sites in Ru/C-120. In summary, the two characteristics correspond to the excellent activity of Ru/C-120, which indicates that high fraction of active sites and low hydrogen desorption peak result in the superior catalytic activity for Ru/C-120. The deconvolution of hydrogen desorption peaks of all Ru/C catalysts are shown in Fig. S5 (Supporting information). Fig. 2f shows that the proportion of H1 peak first decreases and then increases with the particle size increases. The SA shows the same changing trend, suggesting that H1 may contribute most of the HOR activity, and HBE is the main descriptor. Ru/C-120 has the largest proportion of H1 peak, while Ru/C-300 has the smallest proportion of H1 peak.

In addition, OH species binding energy (OHBE) should be considered because Ru has strong oxophilicity, and is generally used to accelerate the removal of H_{ad} to achieve high HOR activities. The potential of CO-stripping provides a sensitive measure of the OHBE, due to CO_{ad} can be removed by the OH_{ad} on the Ru surface [45,46]. CO-stripping curves of all Ru/C catalysts are shown in Fig. S5 (Supporting information). Fig. 3d shows the potential of CO stripping on all Ru/C catalysts first increases, and then decreases with particle size, in which Ru/C-300 have the most positive potential, corresponding to the smallest SA, suggesting that OH_{ad} maybe have some effect on HOR performance.

In order to compare the HER performance of Ru/C catalysts with different particle sizes, LSV testing was conducted in H_2-saturated 1 mol/L KOH using a three-electrode system. Fig. 4a exhibits the HER polarization curves of Ru/C catalysts. The overpotential at 10 mA/cm^2 increased in the order of Ru/C-600 (30 mV) < Ru/C-500 (34 mV) < Ru/C-400 (37 mV) < Ru/C-300 (40 mV) < Ru/C-150 (52 mV) < Ru/C-120 (61 mV) < Ru/C-10 (77 mV). Obviously, Ru/C-600 required the smallest potential of 30 mV to achieve a current density of 10 mA/cm^2, whereas Ru/C-10 required the highest potential of 77 mV. The HER activity of Ru/C catalysts increases with the increasing of the particle size. However, the activity decreases when the annealing temperature reaches above 600 °C, and the overpotential of Ru/C-600 is 30 mV, smaller than 39 mV of Ru/C-700, which is attributed to the increased size of Ru particles. Meanwhile, Ru/C-600 has the highest MA (0.625 A/mg@50 mV), which is 1.3 times of that of Ru/C-700 (0.468 A/mg@50 mV) and 3.7 times of that of Ru/C-10 (0.17 A/mg@50 mV) in Fig. 4b. Furthermore, the HER performance of Ru/C-600 is higher than Pt/C (0.405 A/mg@50 mV) (Fig. S7 in Supporting information). The Tafel plots (Fig. 4c) can be acquired from the HER polarization curves. The Ru/C-600 shows the Tafel slope of 33.7 mV/dec, which is smaller than other Ru/C catalysts, indicating a fast HER kinetics. The Tafel slopes of the Ru/C catalyst is in the range of 20–40 mV/dec, indicating that the path to catalyze HER reaction is Volmer-Tafel process ($H^+ + e^- \rightleftharpoons H_{ads}$, $2H_{ads} \rightleftharpoons H_2$) and the combination of H_{ads} to produce H_2 (Tafel step) is the rate-determining step [47–50]. To deeply underatand the HER activity of Ru/C catalysts, the electrochemical double-layer capacitance (C_{dl}) could be obtained by linear fitting the currents at different scan rates in the non-Faraday zone, is applied to calculate the ECSA. Fig. 4d shows that the C_{dl} of Ru/C-600 is much larger than other Ru/C catalysts, corresponding to the largest number of active sites, explaining its excellent HER activity [51–53].

In general, the catalyst with smaller particle size represents greater degree of metal dispersion, corresponding to more surface active sites [38]. However, it is found that the Ru/C-600 has the largest C_{dl} and the maximum number of active sites, while the particle size of Ru/C catalysts increases and the dispersion reduces with the increase of post-treatment temperature from 10 °C to 600 °C. The HER activity of Ru/C catalyst depends on the surface state (the content of Ru^0) and the particle size of the catalyst

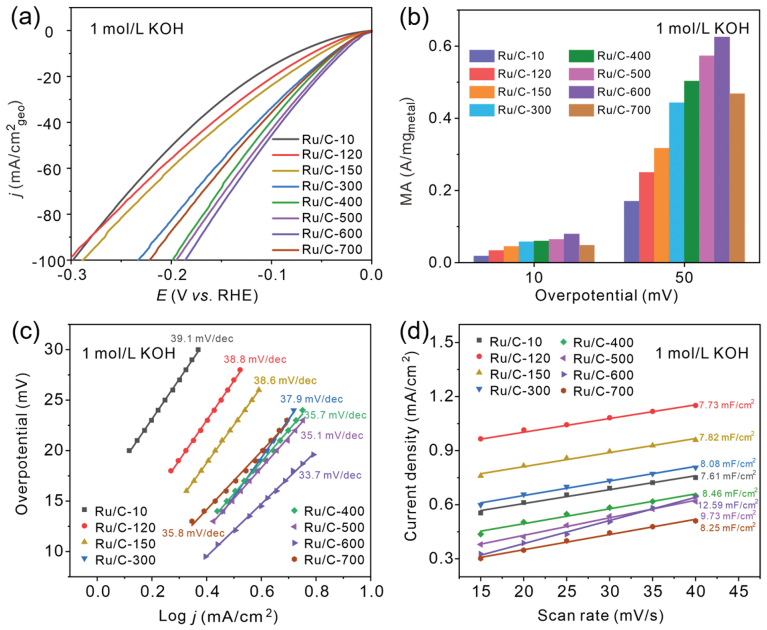

Fig. 4. (a) HER polarization curves of Ru/C-10, Ru/C-120, Ru/C-150, Ru/C-300, Ru/C-400, Ru/C-500, Ru/C-600 and Ru/C-700 in 1 mol/L KOH, (b) the comparison of exchange current density at different overpotentials, (c) corresponding Tafel plots, (d) scan rate dependence of the current densities at 0.195 V.

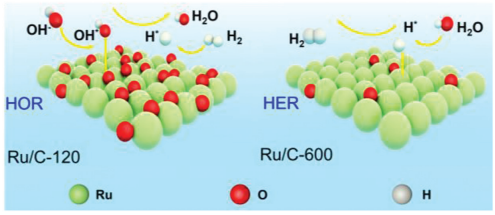

Fig. 5. The schematic illustration of the HOR/HER mechanism on Ru/C-120 and Ru/C-600 catalysts.

(Fig. 5). The Ru/C-600 has the most excellent performance, although its particle size is larger than that of other Ru/C catalysts obtained at lower temperatures. This can be attributed to the fact that the oxygenated species on the surface of Ru/C catalysts obtained at low temperatures would hinder the reaction, while the metallic Ru^0 is the active center for catalyzing HER [30,54]. From the XPS, the ratio of Ru^0 in Ru/C-600 is 65.8%, while Ru/C-10 and Ru/C-120 are 48.4% and 57.4%, respectively. The reason for the poor catalytic performance of Ru/C-700 is related to the increased Ru nanoparticle sizes.

In summary, we found that the HOR and HER activities of Ru/C catalysts are highly correlated with the composition and particle sizes. The metallic Ru^0 is the active site for the hydrogen electrode reaction, while Ru^{x+} would hinder the adsorption and desorption of hydrogen, thereby inhibiting the HOR and HER reactions. The catalysts with smaller particle size can provide more active sites. However, the surface of small Ru particles is easily to form oxygenated species due to the highly instability of Ru. Both the HER and HOR activities of Ru/C show a volcano shaped curve with particle size increasing. Because the HOR is a three-phase interface reaction of gas on the surface of the catalyst, smaller catalyst is benefit to the progress of the reaction. Ru/C-120 has the best HOR activity, while particle size has a great influence. In addition, the deconvolution of hydrogen desorption peak of the Ru/C catalyst found that the proportion of sites with lower HBE is directly related to the HOR activity, which proves that HBE is the descriptor of the HOR reaction. For HER, Ru/C-600 has the best catalytic activity, indicating that the surface state of the catalyst, that is, the ratio of Ru^0 have a great impact on the activity of HER. The results of this experiment provide useful guidance for the subsequent design of Ru-based electrocatalysts.

Declaration of competing interest

The authors declare that they have no known competing financial interests or personal relationships that could have appeared to influence the work reported in this paper.

Acknowledgments

This work was supported by the National Natural Science Foundation (No. 91963109). The authors thank the Analytical and Testing Center of HUST for allowing the use of its help and facilities for XRD, SEM and TEM.

Supplementary materials

Supplementary material associated with this article can be found, in the online version, at doi:10.1016/j.cclet.2022.06.045.

References

[1] L. An, X. Zhao, T. Zhao, et al., Energy Environ. Sci. 14 (2021) 2620–2638.
[2] Y. Zhao, X. Wang, Z. Li, et al., Chin. Chem. Lett. 33 (2022) 1065–1069.
[3] Y. Men, J. Su, X. Wang, et al., Chin. Chem. Lett. 30 (2019) 634–637.
[4] T. Zhao, G. Wang, M. Gong, et al., ACS Catal. 10 (2020) 15207–15216.
[5] W. Sheng, Z. Zhuang, M. Gao, et al., Nat. Commun. 6 (2015) 5848–5854.
[6] W. Sheng, H.A. Gasteiger, Y. Shao-Horn, J. Electrochem. Soc. 157 (2010) 1529–1536.
[7] J. Durst, A. Siebel, C. Simon, et al., Energy Environ. Sci. 7 (2014) 2255–2260.
[8] E.S. Davydova, S. Mukerjee, F. Jaouen, et al., ACS Catal. 8 (2018) 6665–6690.
[9] J. Wang, X. Dong, J. Liu, et al., ACS Catal. 11 (2021) 7422–7428.
[10] J. Wang, J. Liu, B. Zhang, et al., J. Mater. Chem. A 9 (2021) 22934–22942.
[11] W. Sheng, M. Myint, J.G. Chen, et al., Energy Environ. Sci. 6 (2013) 1509–1512.
[12] Y. Zheng, Y. Jiao, Y. Zhu, et al., J. Am. Chem. Soc. 138 (2016) 16174–16181.
[13] N. Danilovic, R. Subbaraman, D. Strmcnik, et al., Angew. Chem. 51 (2012) 12495–12498.
[14] J. Ohyama, D. Kumada, A. Satsuma, J. Mater. Chem. A 4 (2016) 15980–15985.
[15] S. St. John, R.W. Atkinson, R.R. Unocic, et al., J. Phys. Chem. C 119 (2015) 13481–13487.
[16] Y. Xue, L. Shi, X. Liu, et al., Nat. Commun. 11 (2020) 5651–5659.

[17] H.A. Gasteiger, N.M. Markovic, P.N. Ross, J. Phys. Chem. 99 (1995) 16757–16767.
[18] N.M. Markovia, S.T. Sarraf, H.A. Gasteiger, et al., J. Chem. Soc. Faraday Trans. 92 (1996) 3719–3725.
[19] J. Ohyama, T. Sato, Y. Yamamoto, et al., J. Am. Chem. Soc. 135 (2013) 8016–8021.
[20] Y. Zhao, Y. Luo, X. Yang, et al., J. Hazard. Mater. 332 (2017) 124–131.
[21] S.H. Joo, J.Y. Park, J.R. Renzas, et al., Nano Lett. 10 (2010) 2709–2713.
[22] O. Antoine, Y. Bultel, R. Durand, et al., Electrochim. Acta 43 (1998) 3681–3691.
[23] Y. Sun, Y. Dai, Y. Liu, et al., Phys. Chem. Chem. Phys. 14 (2012) 2278–2285.
[24] J. Zheng, Z. Zhuang, B. Xu, et al., ACS Catal. 5 (2015) 4449–4455.
[25] J. Zheng, S. Zhou, S. Gu, et al., J. Electrochem. Soc. 163 (2016) 499–506.
[26] M. Gong, J. Zhu, M. Liu, et al., Nanoscale 11 (2019) 20301–20306.
[27] Y. Zhao, X. Wang, G. Cheng, et al., ACS Catal. 10 (2020) 11751–11757.
[28] H. Song, M. Wu, Z. Tang, et al., Angew. Chem. Int. Ed. 60 (2021) 7234–7244.
[29] T. Li, H. Lin, X. Ouyang, et al., ACS Catal. 9 (2019) 5828–5836.
[30] J. Wang, Z. Wei, S. Mao, et al., Energy Environ. Sci. 11 (2018) 800–806.
[31] K. Qadir, S.H. Joo, B.S. Mun, et al., Nano Lett. 12 (2012) 5761–5768.
[32] S. Mao, C. Wang, Y. Wang, J. Catal. 375 (2019) 456–465.
[33] K. Kusada, H. Kobayashi, R. Ikeda, et al., J. Am. Chem. Soc. 136 (2014) 1864–1871.
[34] L. Zeng, H. Peng, W. Liu, et al., J. Power Sources 461 (2020) 228147–228154.
[35] Y. Li, J. Abbott, Y. Sun, et al., Appl. Catal. B 258 (2019) 117952.
[36] H. Inoue, J.X. Wang, K. Sasaki, et al., J. Electroanal. Chem. 554-555 (2003) 77–85.
[37] C. Xu, M. Mei, Q. Wang, et al., J. Mater. Chem. A 6 (2018) 14380–14386.
[38] Y.J. Wang, N. Zhao, B. Fang, et al., Chem. Rev. 115 (2015) 3433–3467.
[39] H. Wang, H.D. Abruna, J. Am. Chem. Soc. 139 (2017) 6807–6810.
[40] S. St. John, R.W. Atkinson, K.A. Unocic, et al., ACS Catal. 5 (2015) 7015–7023.
[41] Y. Cong, B. Yi, Y. Song, Nano Energy 44 (2018) 288–303.
[42] M.A. Lukowski, A.S. Daniel, F. Meng, et al., J. Am. Chem. Soc. 135 (2013) 10274–10277.
[43] J. Zheng, J. Nash, B. Xu, et al., J. Electrochem. Soc. 165 (2018) 27–29.
[44] T. Zhao, D. Xiao, Y. Chen, et al., J. Energy Chem. 61 (2021) 15–22.
[45] Y. Wang, G. Wang, G. Li, et al., Energy Environ. Sci. 8 (2015) 177–181.
[46] L. Zhuang, J. Jin, H.D. Abruña, J. Am. Chem. Soc. 129 (2007) 11033–11035.
[47] Y. Liu, X. Li, Q. Zhang, et al., Angew. Chem. 59 (2020) 1718–1726.
[48] Y. Liu, Q. Feng, W. Liu, et al., Nano Energy 81 (2021) 105641.
[49] Q. Zhou, Q. Bian, L. Liao, et al., Chin. Chem. Lett. 34 (2023) 107248.
[50] J. Zeng, L. Zhang, Q. Zhou, et al., Small 18 (2022) e2104624.
[51] M. Caban-Acevedo, M.L. Stone, J.R. Schmidt, et al., Nat. Mater. 14 (2015) 1245–1251.
[52] D. Li, L. Liao, H. Zhou, et al., Mater. Today Phys. 16 (2021) 100314.
[53] Q. Zhou, L. Liao, Q. Bian, et al., Small 18 (2022) e2105642.
[54] E. Demir, S. Akbayrak, A.M. Onal, et al., J. Colloid Interface Sci. 531 (2018) 570–577.